

# Machine Learning Enhanced Quantum State Tomography on FPGA

Hsun-Chung Wu,<sup>1</sup> Hsien-Yi Hsieh,<sup>1</sup> Zhi-Kai Xu,<sup>2</sup> Hua Li Chen,<sup>3</sup> Zi-Hao Shi,<sup>1</sup> Po-Han Wang,<sup>1</sup> Popo Yang,<sup>1</sup> Ole Steuernagel,<sup>1</sup> Chien-Ming Wu,<sup>1</sup> and Ray-Kuang Lee<sup>1,2,3,4,5\*</sup>

<sup>1</sup>*Institute of Photonics Technologies, National Tsing Hua University, Hsinchu 30013, Taiwan*

<sup>2</sup>*Department of Electrical Engineering, National Tsing Hua University, Hsinchu 30013, Taiwan*

<sup>3</sup>*Department of Physics, National Tsing Hua University, Hsinchu 30013, Taiwan*

<sup>4</sup>*Center for Theory and Computation, National Tsing Hua University, Hsinchu 30013, Taiwan*

<sup>5</sup>*Center for Quantum Science and Technology, Hsinchu 30013, Taiwan*

(Dated: January 9, 2025)

Machine learning techniques have opened new avenues for real-time quantum state tomography (QST). In this work, we demonstrate the deployment of machine learning-based QST onto edge devices, specifically utilizing field programmable gate arrays (FPGAs). This implementation is realized using the *Vitis AI Integrated Development Environment* provided by AMD<sup>®</sup> Inc. Compared to the Graphics Processing Unit (GPU)-based machine learning QST, our FPGA-based one reduces the average inference time by an order of magnitude, from 38 ms to 2.94 ms, but only sacrifices the average fidelity about 1% reduction (from 0.99 to 0.98). The FPGA-based QST offers a highly efficient and precise tool for diagnosing quantum states, marking a significant advancement in the practical applications for quantum information processing and quantum sensing.

## I. INTRODUCTION

Accurately characterizing the full information in a quantum system is a critical challenge in the presence of unavoidable environmental noises. Quantum state tomography (QST), particularly through balanced homodyne measurements, has become an essential tool for reconstructing quantum states, serving as a diagnostic method in many applications [1, 2]. Starting with the maximum likelihood estimation (MLE) [3–5], QST has been widely applied to not only discrete and continuous variables, but also the hybrid ones in optical, atomic, ionic, semiconductor and superconducting systems [6–13].

With recent advances in artificial intelligence (AI), computational hardware have enabled the application of machine learning (ML) techniques to various sub-fields both in the classical and quantum world. To enhance the efficiency in applying QST, ML-enhanced QST has provided the solutions to overcome the limitations in using conventional QST algorithms, such as overfitting and long run-time problems [14–16]. For example, in Ref. [17], we have demonstrated the potential of using ML to improve QST by framing it as a feature parameter estimation problem, reducing the model complexity by skipping the computationally expensive process in reconstructing density matrix. Even though hybrid quantum-classical neural networks or fully quantum neural networks are still evolving towards promising quantum machine learning architectures [18–20], edge devices are already available for applications in resource-limited computational environments.

In this work, we implement the ML-enhanced QST on edge computing devices, i.e., the field programmable gate array (FPGA) from AMD<sup>®</sup> *ZCU104 Evaluation Board*, by deploying a parameter estimation neural network model. As a configurable integrated circuit with flexibility, high signal processing speed, and parallel processing capabilities, FPGA

have been widely used in various industrial sectors such as telecommunications, automotive, and aerospace. Benchmarking with our Graphics Processing Unit (GPU)-based ML-enhanced QST [15, 17], a significant reduction in the average inference time is demonstrated, from 38 ms to 2.94 ms. At the same time, our FPGA only lower the output average fidelity from 0.99 to 0.98, verifying a trustable reconstruction model. With these experimental results, our ML-enhanced QST on FPGA leverages simplicity and efficiency to facilitate real-time quantum state analysis in resource-limited computational environments.

This paper is organized as follows: in Sec. II, we introduce the flow charts of our implementation on ML-enhanced QST onto a FPGA device. Then, in Sec. III, comparisons between GPU-based and FPGA-based ML-enhanced QST, for average fidelity and run-time costs are reported. Some further perspectives are provided, before we, finally, conclude this paper in Sec. VI.

## II. IMPLEMENTATION FLOW CHART

In Fig. 1, we show the schematic of our FPGA-based QST. Here, the AMD<sup>®</sup> *ZCU104 Evaluation Board* is our FPGA device. The overall picture is to feed the input quadrature sequence from homodyne signal into a FPGA. Then, based on our deployed QST algorithm (see below for the flow charts on how to implement it), the FPGA generates the state parameters to reconstruct the density matrix, Wigner function, or the characteristics (such as the average photon number) accordingly.

Regarding the implementation process of ML-enhanced QST on FPGA, in Fig. 2, we use a diagram of flow charts to outline each step.

In edge devices, computational resource limitations often lead to challenges in maintaining precision. For the implementation, we first utilize the package “tf.keras” to export the off-line, pre-trained neural network we have in Ref. [17], from the format with FP32 precision into a “.h5”-formatted file. To

\* rkleee@ee.nthu.edu.tw

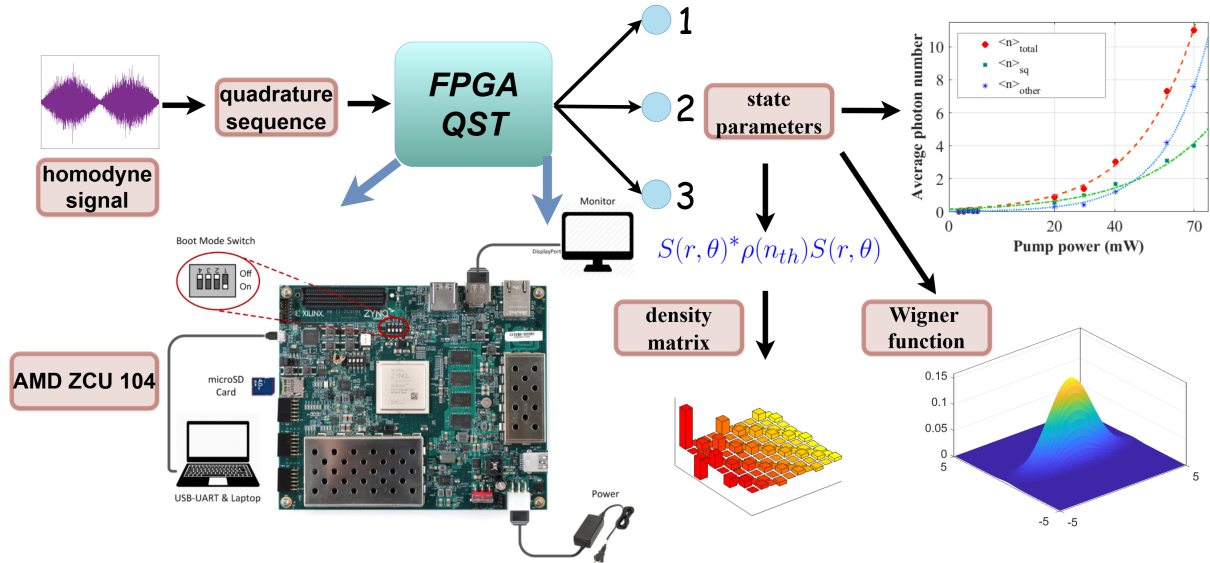


FIG. 1. Schematic of our FPGA quantum state tomography (QST), with the input quadrature sequence from homodyne signal, which generates the state parameters to reconstruct the density matrix, Wigner function, or characteristics (such as the average photon number) accordingly.

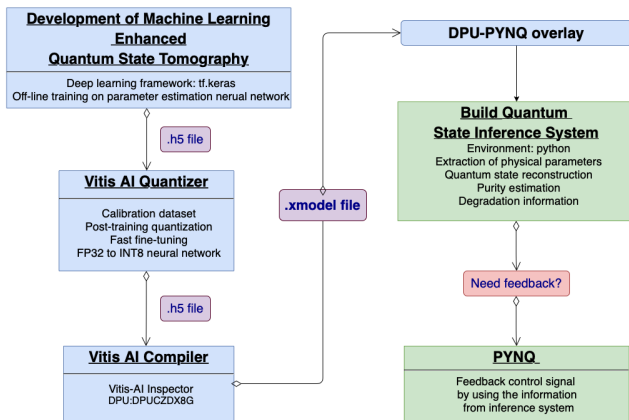


FIG. 2. Flow charts of our implementation of ML-enhanced QST on FPGA.

mitigate this, we optimized our INT8 machine learning model using *Vitis AI* provided by AMD<sup>®</sup> Inc.

Subsequently, we employ the *Vitis AI Integrated Development Environment* to convert the neural network from the format of FP32 floating-point numbers to the INT8 format, and generate the “.xmodel file” for a specific FPGA with ML algorithm. The *Vitis AI Integrated Development Environment* provides AI inference on AMD<sup>®</sup> (and Xilinx<sup>®</sup>) hardware platforms [21]. First, with the *Vitis AI Quantizer*, our machine learning model is converted into an integer format (INT8) for efficient storage and computation. Then, the *Vitis AI Compiler* is employed to transform the quantized model into the model file, i.e., in the format of “.xmodel” file, which is compatible with FPGA deployment. The compiler optimizes the model based on the hardware architecture, as well as the layout of FPGA used, invoking appropriate IP (Intellectual Property)

cores for computation.

The framework of the *Vitis AI Development Environment* mainly includes *Vitis AI Quantizer*, *Vitis AI Compiler* and DPU (Deep learning Processing Unit) parts, respectively. Briefly, we summarize these three parts.

*Vitis AI Quantizer*: During the training phase of the neural network, 32-bit floating point weights and activation values are used. The function of the *Vitis AI Quantizer* is to convert 32-bit floating point weights and activations into 8-bit integer (INT8) format. This uses fewer overheads whilst maintaining prediction accuracy. In fact, the fixed-point network model requires less memory bandwidth and is proven to provide higher speeds and greater power efficiency than the floating-point model. Additionally, the *Vitis AI Quantizer* can be executed in common layers of neural networks, such as convolutional layers, pooling layers, fully connected layers, etc.

During the quantization process, we prepare 1,000 quadrature sequences as a calibration dataset, with each sequence containing 2,048 quadrature values. We also apply the so-called ‘post-training quantization’, to fine-tune and optimize model performance.

*Vitis AI Compiler*: The *Vitis AI Compiler* takes a ‘quantized’ neural network model (FP32 to INT8) as input and compiles it into a format that a specific DPU can read (the IP for our edge device *ZCU104 Evaluation Board* is *DPUCZDX8G*). The compiler accepts quantized models processed by the relevant language: *Caffe*, *TensorFlow* or *PyTorch*. Finally, it is converted into a compiled “.xmodel” file.

*Deep learning Processing Unit (DPU)*: The DPU is an IP core specifically designed to accelerate deep learning inference on FPGAs. Here, an IP core is a pre-designed,

pre-verified module used in electronic circuit design. IP is usually written in *Verilog*<sup>®</sup> or *VHDL*<sup>®</sup> languages. By writing in these programming languages, one can control the programmable logic embedded in FPGA into specific logic configurations, such as adders or decoders. IP cores provide specific functions or tasks to be integrated directly into an FPGA. Using IP cores helps designers save time and focus on the unique aspects of their projects.

After using the *Vitis AI Integrated Development Environment* to convert the INT8 model into a specialized “.xmodel” format, we can use this to off-load the corresponding DPU and transform our integer model into an appropriate FPGA computing unit for execution. We want to remark that before this conversion, we also utilized the *Vitis AI* inspector to verify that each component and structure of our neural network is supported by the DPU.

Different FPGA boards have different architectures, hence, different DPU modules correspond to each architecture. The *Vitis AI Integrated Development Environment* automatically invokes the appropriate hardware design, generating configuration files based on the FPGA board used, along with the selected DPU model. These files contain pre-designed hardware descriptions and configuration data.

Specifically, we use the edge device *ZCU104 Evaluation Board* as an embedded deep learning processing unit to develop the deep neural networks. The *ZCU104 Evaluation Board* is based on AMD<sup>®</sup> (and Xilinx<sup>®</sup>) FPGA chip, Zynq<sup>®</sup> UltraScale+TM MPSoC. The *ZCU104* can run the *Python* language (also in a *Jupyter Notebook* environment). Additionally, AMD<sup>®</sup> has developed an operating system called *PYNQ* (*DPU-PYNQ* is one of their flavors), which starts the development board by installing *PYNQ* on the SD (Secure Digital) card. The SD card can be directly inserted into the development board allowing the latter to operate independently of a host computer.

For *ZCU104 Evaluation Board*, the *Vitis AI Integrated Development Environment* provides us with an IP core: *DPUCZDX8G*, which allows developers to focus on high-level deep learning model design without delving into the intricacies of underlying hardware implementations.

After uploading the “.xmodel” file to the FPGA board *ZCU104 Evaluation Board*, we use *DPU-PYNQ* [22] for loading the model and employing overlay technology to operate the model. The *DPU-PYNQ* package is provided by Xilinx<sup>®</sup>, which facilitates the deployment and execution of deep learning models on FPGA platforms by using the *PYNQ* framework. It leverages the DPU overlay to enable an efficient inference from neural networks. This package allows users to integrate hardware acceleration into their *Python*-based workflows, enhancing computational performance for machine learning tasks.

In *DPU-PYNQ*, an “overlay” is a high-level concept in FPGA design, representing a hardware configuration that can be dynamically loaded onto the FPGA. An overlay includes predefined hardware, specific IP cores, and connection logic, allowing users to perform specific tasks. On the *PYNQ* platform, overlays consist of a bitstream file and software drivers,

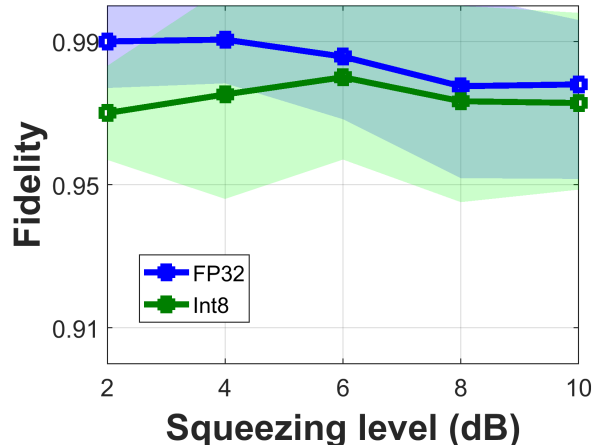


FIG. 3. Comparison of the average output fidelity between GPU-based (original model used in Ref. [15, 17] and FPGA-based (with the Int8 model on the FPGA board: *ZCU 104 Evaluation Board*) ML-enhanced QST, to different squeezing levels in the unite of (dB). The corresponding standard deviations are shown by the shadowed region.

enabling control through *Python* code. This simplifies the development process, as users can deploy and run deep learning inference workloads without deep hardware knowledge. Overlays offer flexibility, simplified development, and quick deployment, making it easy to add new features or update existing ones. Once the model is successfully loaded onto the FPGA, we develop a *Python*-based program to implement a quantum state inference system.

For the deployment and execution of the model on the FPGA, we leverage the *DPU-PYNQ* package [22], which facilitates the integration and loading from the input model onto the hardware. Here, this package processes the experimental data providing input quadrature sequences through a machine learning model to estimate three key parameters. They are the degradation information in the target quantum states, including the quantum state reconstruction, extraction of physical parameters, and purity estimation [15, 17]. These parameters are crucial for calculating the degradation information of squeezed states and can also be used to reconstruct the density matrix or Wigner functions of input quantum states. Last but not least, after deploying the model on such edge devices, if feedback control is desired, this can be achieved through *PYNQ* by reading information obtained from quantum state tomography and controlling the FPGA board to put out signals, e.g., for feedback control purposes.

### III. PERFORMANCE AND RESULTS

We teste our implementation with 100,000 quadrature sequence signals, which are mock data representing degraded squeezed states with various average photon numbers and different squeezing factors. In Fig. 3, we compare the average output fidelity (in solid curves), and the corresponding stan-

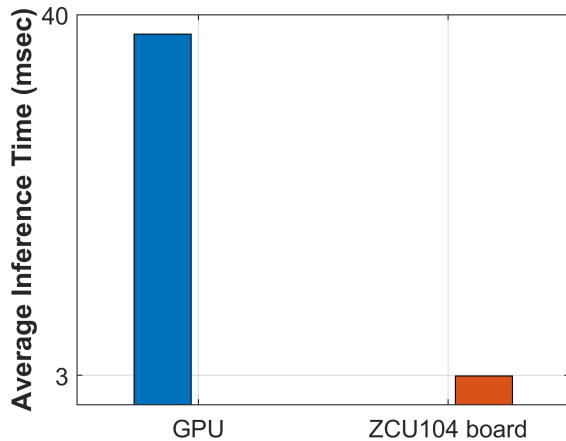


FIG. 4. Comparison of the average inference time cost in milliseconds (msec) between GPU-based and FPGA-based (on *ZCU 104 Evaluation Board*) ML-enhanced QST.

dard deviation shown by the shadowed region, between GPU-based (original model used in Ref. [15, 17]) and FPGA-based (with the Int8 model on the FPGA board: *ZCU 104 Evaluation Board*) ML-enhanced QST. The results clearly demonstrate that the output average fidelity is slightly sacrificed, approximately 1% (e.g., from 0.99 to 0.98).

After confirming that this fidelity reduction is acceptable, we further evaluate the output performance by loading 10,000 quadrature sequence data sets into our custom inference system to measure the average time required for quantum state inference, as shown in Fig. 4. The results demonstrate a significant, namely tenfold, reduction of the inference times (from 38 ms to 2.94 ms). This clearly demonstrates the main benefit of deploying FPGA-based ML-enhanced QST.

Here, we use FPGA-based QST to directly generate characteristic parameters. Specifically, we calculate the average photon number of the pure state, the total average photon number, and the average photon number of the non-pure state (arising from the environment), which enable a clear distinction between contributions from the quantum system and environment. To visualize the density matrix, we also utilize the on-board *Python* and *NumPy* environment to construct the squeezing operator in the Fock basis. Subsequently, one can generate the corresponding density matrix of lossy squeezed states. On the contrary, performing such numerical computations on the FPGA board tends to be slower and is generally not recommended. The demonstrations shown in Fig. 1 are only to illustrate the achievability of this process on the FPGA board.

Moreover, in Fig. 5, we also study the power consumption in our FPGA-based QST. Power consumption is measured using an on-chip current sensor. As one can see, before our QST starts, the power consumption from FPGA is at the power level about 14 Watts, i.e., the Idle Mode shown in Yellow colors. It is known that any program written in *Verilog* or *HDL* using the Vivado IDE (Integrated Development Environment) must be in the format of “bitstream”, for FPGA to load and

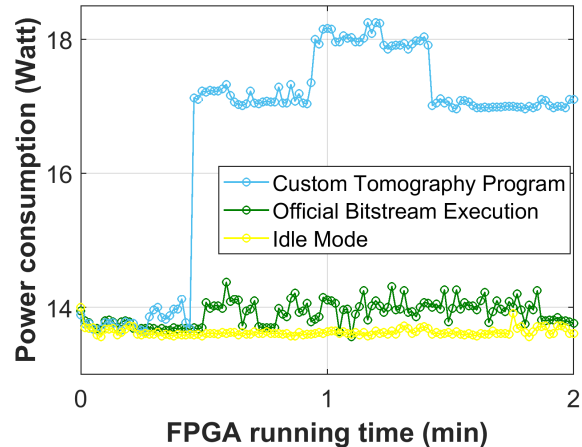


FIG. 5. Power consumption in performing a custom tomography program, i.e., our FPGA-based QST, in loading 10,000 data sets.

execute. Then, the curve in Green colors represents the monitored power consumption during the process of downloading a test bitstream file into the PL (Programmable Logic) region on the FPGA board. The test bitstream file used in this demonstration is provided by AMD<sup>®</sup> Inc. For this official bitstream execution, i.e., the default one, a slight increment in the power consumption is recorded in Green colors. When our program starts to execute, at this point, the power consumption jumps to 17 Watts from the Idle Mode. Then, we load 10,000 quadrature sequence data sets into the FPGA. From this point on, the power consumption increases from 17W to 18W. The total executive duration is about 30 seconds, which is in agreement to the average inference time, i.e.,  $10,000 \times 2.94 \text{ ms} \approx 30 \text{ secs}$  in total. Finally, after finish the QST task the power consumption goes back to 17 Watts.

Furthermore, our neural network model, i.e., the “.xmodel” file compiled by *Vitis AI Compiler*, has been loaded by a *Python* program running in a *Jupyter Notebook* environment to perform AI operations. The *ZCU 104 Evaluation Board* also has built-in wideband I/O connectors and various *Python* packages that can be executed in *Jupyter Notebooks*. One may use *PYNQ* to perform the Proportional-Integral-Derivative (PID) feedback control on the board. We may also connect ADC/DAC cards or sensors (temperature, light, etc.) and obtain signals from the controlled system through *Python* commands. In addition, the *Python* package, e.g., *Matplotlib* in *Jupyter Notebook*, can display input signals on the screen in real time. This helps us achieve a real-time PID feedback control from our FPGA-based ML-enhanced QST.

Through this implementation process, we have successfully deployed quantum state tomography on an FPGA, highlighting the effectiveness of this approach in achieving real-time, high-precision quantum state analysis on resource-constrained devices. In the literature, a scalable and self-analyzing digital locking system is reported for use on quantum optics experiments [23]. An open-source platform, *NQontrol*, is also demonstrated for digital control-loops [24], as well as a reconfigurable QST solver in FPGA [25]. Such a



FPGA-based ML-enhanced QST can be used as an in-line diagnostic toolbox for various applications that rely on the use of squeezed states [26–28]

#### IV. CONCLUSIONS

By using *ZCU 104 Evaluation Board* with the *Vitis AI Integrated Development Environment*, we have successfully deployed machine learning-based quantum state tomography onto a FPGA device, with a slight reduction in the output average fidelity, i.e., from 0.99 to 0.98. But the signal processing speed when reconstructing quantum state from tomography is demonstrated to be 10 times higher, taking 2.94 ms, instead 38 ms previously. With the flexibility and parallel processing abilities, our FPGA-based QST offers a highly efficient and

precise tool toward real-time diagnostics of quantum states. In addition to application to Gaussian states, as illustrated here, this technology paves the way to dealing with more general quantum states, including non-Gaussian states and multipartite quantum states at high through-put speeds.

#### ACKNOWLEDGEMENTS

This work is partially supported by the Ministry of Science and Technology of Taiwan (Nos 112-2123-M-007-001, 112-2119-M-008-007, 112-2119-M-007-006), Office of Naval Research Global, the International Technology Center Indo-Pacific (ITC IPAC) and Army Research Office, under Contract No. FA5209-21-P-0158, and the collaborative research program of the Institute for Cosmic Ray Research (ICRR) at the University of Tokyo.

- 
- [1] U. Leonhardt, *Measuring the Quantum State of Light*, (Cambridge University Press, 1997).
- [2] A. I. Lvovsky and M. G. Raymer, “Continuous-variable optical quantum-state tomography,” *Rev. Mod. Phys.* **81**, 299 (2009).
- [3] K. Banaszek, “Maximum-likelihood estimation of photon-number distribution from homodyne statistics,” *Phys. Rev. A* **57**, 5013 (1998).
- [4] Z. Hradil, “Quantum-state estimation,” *Phys. Rev. A* **55**, R1561(R) (1997).
- [5] A. I. Lvovsky, “Iterative maximum-likelihood reconstruction in quantum homodyne tomography,” *J. Opt. B: Quant. Semiclass. Opt.* **6**, S556 (2004).
- [6] U. L. Andersen, J. S. Neergaard-Nielsen, P. van Loock, and A. Furusawa, “Hybrid discrete- and continuous-variable quantum information,” *Nature Phys.* **11**, 713 (2015).
- [7] D. Barredo, S. de Leseleuc, V. Lienhard, T. Lahaye, and A. Browaeys, “An atom-by-atom assembler of defect-free arbitrary two-dimensional atomic arrays,” *Science* **354**, 1021 (2016).
- [8] M. Endres, H. Bernien, A. Keesling, H. Levine, E. R. Anschuetz, A. Krajenbrink, C. Senko, V. Vuletic, M. Greiner, and M. D. Lukin, “Atom-by-atom assembly of defect-free one-dimensional cold atom arrays,” *Science* **354**, 1024 (2016).
- [9] J. Zhang, G. Pagano, P. W. Hess, A. Kyprianidis, P. Becker, H. Kaplan, A. V. Gorshkov, Z.-X. Gong, and C. Monroe, “Observation of a many-body dynamical phase transition with a 53-qubit quantum simulator,” *Nature* **551**, 601 (2017).
- [10] N. Friis, O. Marty, C. Maier, C. Hempel, M. Holzäpfel, P. Jurcevic, M. B. Plenio, M. Huber, C. Roos, R. Blatt, and B. Lanyon, “Observation of entangled states of a fully controlled 20-qubit system,” *Phys. Rev. X* **8**, 021012 (2018).
- [11] D. Cogan, G. Peniakov, Z.-E. Su, and D. Gershoni, “Complete state tomography of a quantum dot spin qubit,” *Phys. Rev. B* **101**, 035424 (2020).
- [12] K. Takeda, A. Noiri, T. Nakajima, J. Yoneda, T. Kobayashi, and S. Tarucha, “Quantum tomography of an entangled three-qubit state in silicon,” *Nature Nano.* **16**, 965 (2021).
- [13] B. Vlastakis, G. Kirchmair, Z. Leghtas, S. E. Nigg, L. Frunzio, S. M. Girvin, M. Mirrahimi, M. H. Devoret, and R. J. Schoelkopf, “Deterministically encoding quantum information using 100- photon Schrödinger cat states,” *Science* **342**, 607 (2013).
- [14] E. S. Tiunov, V. V. Tiunova, A. E. Ulanov, A. I. Lvovsky, and A. K. Fedorov, “Experimental quantum homodyne tomography via machine learning,” *Optica* **7**, 448 (2020).
- [15] H.-Y. Hsieh, Y.-R. Chen, H.-C. Wu, H. L. Chen, J. Ning, Y.-C. Huang, C.-M. Wu, and R.-K. Lee, “Extract the Degradation Information in Squeezed States with Machine Learning,” *Phys. Rev. Lett.* **128**, 073604 (2022).
- [16] S. Ahmed, C. S. Muoz, F. Nori, and A. F. Kockum, “Quantum State Tomography with Conditional Generative Adversarial Networks,” *Phys. Rev. Lett.* **127**, 140502 (2021).
- [17] H.-Y. Hsieh, J. Ning, Y.-R. Chen, H.-C. Wu, H. L. Chen, C.-M. Wu, and R.-K. Lee, “Direct parameter estimations from machine learning-enhanced quantum state tomography,” *Symmetry*, **14**, 874, (2022).
- [18] J. Biamonte, P. Wittek, N. Pancotti, P. Rebentrost, N. Wiebe, and S. Lloyd, “Quantum machine learning,” *Nature* **549**, 195 (2017).
- [19] S. Lohani, B. T. Kirby, M. Brodsky, O. Danaci, and R. T. Glasser, “Machine learning assisted quantum state estimation,” *Mach. Learn.: Sci. Technol.* **1**, 035007 (2020).
- [20] A. Melnikov, M. Kordzanganeh, A. Alodjants, and R.-K. Lee, “Quantum Machine Learning: from physics to software engineering,” *Advances in Phys. X* **8**, 2165452 (2023).
- [21] AMD<sup>®</sup> Inc. *Vitis AI User Guide*. UG1414 (v3.0) Feb. 24, (2023).
- [22] AMD<sup>®</sup> Inc. *DPUCZDX8G for Zynq<sup>®</sup>UltraScale+ MPSoC*. PG338 (v4.1) Jan. 23, (2023).
- [23] B. M. Sparkes, H. M. Chrzanowski, D. P. Parrain, B. C. Buchler, P. K. Lam, and T. Symul, “A scalable, self-analyzing digital locking system for use on quantum optics experiments,” *Rev. Sci. Instrum.* **82**, 075113 (2011).
- [24] C. Darsow-Fromm, L. Dekant, S. Grebien, M. Schröder, R. Schnabel, and S. Steinlechner, “NQontrol: An open-source platform for digital control-loops in quantum-optical experiments,” *Rev. Sci. Instrum.* **91**, 035114 (2020).
- [25] N. E. Miller, B. Chakraborty and S. Mukhopadhyay, “A Reconfigurable Quantum State Tomography Solver in FPGA,” 2023 IEEE International Conference on Quantum Computing and Engineering (QCE), Bellevue, WA, USA, 2023, pp. 1412-1421.
- [26] Y.-R. Chen, H.-Y. Hsieh, J. Ning, H.-C. Wu, H. L. Chen, Y.-L. Chuang, P. Yang, O. Steuernagel, C.-M. Wu, and R.-K. Lee,

- “Experimental reconstruction of Wigner phase-space current,” *Phys. Rev. A* **108**, 023729 (2023).
- [27] Y.-R. Chen, H.-Y. Hsieh, J. Ning, H.-C. Wu, H. L. Chen, Z.-H. Shi, P. Yang, O. Steuernagel, C.-M. Wu, and R.-K. Lee, “Generation of heralded optical cat states by photon addition,” *Phys. Rev. A* **110**, 023703 (2024).
- [28] H.-Y. Hsieh, Y.-R. Chen, J. Ning, H.-C. Wu, H. L. Chen, Z.-H. Shi, P.-H. Wang, O. Steuernagel, C.-M. Wu, and R.-K. Lee, “Neural-network-enhanced Fock-state tomography,” *Phys. Rev. A* **110**, 053705 (2024).